J|A|C|S
ARTICLES
Published on Web 04/08/2005

Multifunctionality and Crystal Dynamics of a Highly Stable, Porous Metal−Organic Framework [$Zn_4O(NTB)_2$]

Eun Young Lee, Seung Yeon Jang, and Myunghyun Paik Suh*

Contribution from the Department of Chemistry, Seoul National University, Seoul 151-747, Republic of Korea

Received October 14, 2004; E-mail: mpsuh@snu.ac.kr

Abstract: A porous metal−organic framework [$Zn_4O(NTB)_2$]·3DEF·EtOH (**1**), in which (3,6)-connected nets are doubly interpenetrated to generate curved three-dimensional channels, has been prepared. Framework **1** exhibits high permanent porosity (Langmuir surface area, 1121 m^2/g; pore volume, 0.51 cm^3/cm^3), high thermal stability (up to 430 °C), high hydrogen adsorption capacity (1.9 wt % at 77 K and 1 atm), selective organic guest binding ability (K_f: MeOH > pyridine > benzene > dodecane), and guest-dependent blue luminescence (λ_{max} depending on guest identity). Most interestingly, the framework sustains single crystallinity even at 400 °C and 10^{-5} Torr, and the framework components undergo reversible dynamics, mainly *rotational motion*, in response to removal and rebinding of the guest molecules.

Introduction

Metal−organic open frameworks (MOFs) having diverse architectures and functions have been assembled from molecular building blocks.[1−16] They have potential to be applied to molecular adsorption and separation processes,[1,2,10,13,15] ion-exchange,[4a,17] catalysis,[18,19] sensor technology,[20−22] and opto-electronics.[23] Despite the extensive studies, application of MOFs is still quite limited compared to that of zeolites. This is because (i) they often collapse when the guest molecules occupying the voids are removed even though considerable numbers of porous MOF are robust,[12−15] (ii) they frequently dissociate into the building blocks on immersion in solvents,[1−4] and (iii) they are, in general, thermally unstable compared with inorganic zeolites and are destroyed at high temperatures (>300 °C) or even at low temperatures under vacuum. In particular, frameworks showing simultaneously permanent porosity, high thermal stability, and luminescence are extremely rare.[16] Some MOFs showing crystal-to-crystal transformation[1,5−8,11−14,24,25] or novel phenomena of crystal dynamics[1,6,7,24] have been reported, but such MOFs are still not very common.

Here we report the multifunctionality and crystal dynamics of the metal−organic open framework, [$Zn_4O(NTB)_2$]·3DEF·EtOH (**1**) (DEF = *N*,*N*′-diethylformamide), which has been prepared by the solvothermal reaction of $Zn(NO_3)_2·6H_2O$ and 4,4′,4″-nitrilotrisbenzoic acid (H_3NTB) in DEF/EtOH/H_2O (5:3:2, v/v).[26] **1** exhibits permanent porosity with greater pore

(1) (a) Suh, M. P.; Ko, J. W.; Choi, H. J. *J. Am. Chem. Soc.* **2002**, *124*, 10976−10977. (b) Choi, H. J.; Suh, M. P. *J. Am. Chem. Soc.* **2004**, *126*, 15844−15851.
(2) (a) Choi, H. J.; Suh, M. P. *J. Am. Chem. Soc.* **1998**, *120*, 10622−10628. (b) Choi, H. J.; Lee, T. S.; Suh, M. P. *Angew. Chem., Int. Ed.* **1999**, *38*, 1405−1408. (c) Ko, J. W.; Min, K. S.; Suh, M. P. *Inorg. Chem.* **2002**, *41*, 2151−2157.
(3) (a) Min, K. S.; Suh, M. P. *Chem. Eur. J.* **2001**, *7*, 303−313. (b) Suh, M. P.; Choi, H. J.; So, S. M.; Kim, B. M. *Inorg. Chem.* **2003**, *42*, 676−678.
(4) (a) Min, K. S.; Suh, M. P. *J. Am. Chem. Soc.* **2000**, *122*, 6834−6840. (b) Choi, H. J.; Suh, M. P. *Inorg. Chem.* **1999**, *38*, 6309−6312.
(5) Biradha, K.; Hongo, Y.; Fujita, M. *Angew. Chem., Int. Ed.* **2000**, *39*, 3843−3845.
(6) Biradha, K.; Fujita, M. *Angew. Chem., Int. Ed.* **2002**, *41*, 3392−3395.
(7) Biradha, K.; Hongo, Y.; Fujita, M. *Angew. Chem., Int. Ed.* **2002**, *41*, 3595−3598.
(8) Abrahams, B. F.; Jackson, P. A.; Robson, R. *Angew. Chem., Int. Ed.* **1998**, *37*, 2656−2659.
(9) Kitagawa, S.; Kitaura, R.; Noro, S. *Angew. Chem., Int. Ed.* **2004**, *43*, 2334−2375.
(10) (a) Kitaura, R.; Noro, S.; Kondo, M.; Kitagawa, S. *Angew. Chem., Int. Ed.* **2002**, *41*, 133−135. (b) Kitaura, R.; Seki, K.; Akiyama, G.; Kitagawa, S. *Angew. Chem., Int. Ed.* **2003**, *42*, 428−431.
(11) Rather, B.; Zaworotko, M. J. *Chem. Commun.* **2003**, 830−831.
(12) Chui, S. S.-Y.; Lo, S. M.-F.; Charmant, J. P. H.; Orpen, A. G.; Williams, I. D. *Science* **1999**, *283*, 1148−1150.
(13) Lee, E. Y.; Suh, M. P. *Angew. Chem., Int. Ed.* **2004**, *43*, 2798−2801.
(14) (a) Eddaoudi, M.; Moler, D. B.; Li, H.; Chen, B.; Reineke, T. M.; O'Keeffe, M.; Yaghi, O. M. *Acc. Chem. Res.* **2001**, *34*, 319−330. (b) Chen, B.; Eddaoudi, M.; Reineke, T. M.; Kampf, J. W.; O'Keeffe, M.; Yaghi, O. M. *J. Am. Chem. Soc.* **2000**, *122*, 11559−11560.
(15) (a) Eddaoudi, M.; Li, H.; Yaghi, O. M. *J. Am. Chem. Soc.* **2000**, *122*, 1391−1397. (b) Li, H.; Eddaoudi, M.; O'Keeffe, M.; Yaghi, O. M. *Nature* **1999**, *402*, 276−279. (c) Eddaoudi, M.; Kim, J.; Rosi, N.; Vodak, D.; Watcher, J.; O′Keeffe, M.; Yaghi, O. M. *Science* **2002**, *295*, 469−472. (d) Yaghi, O. M.; O'Keeffe, M.; Ockwig, N. W.; Chae, H. K.; Eddaoudi, M.; Kim, J. *Nature* **2003**, *423*, 705−714. (e) Rosi, N. L.; Eckert, J.; Eddaoudi, M.; Vodak, D. T.; Kim, J.; O'Keeffe, M.; Yaghi, O. M. *Science* **2003**, *300*, 1127−1129.
(16) Reineke, T. M.; Eddaoudi, M.; Fehr, M.; Kelley, D.; Yaghi, O. M. *J. Am. Chem. Soc.* **1999**, *121*, 1651−1657.
(17) Yaghi, O. M.; Li, H. *J. Am. Chem. Soc.* **1996**, *118*, 295−296.
(18) Seo, J. S.; Whang, D.-M.; Lee, H.-Y.; Jun, S. I.; Oh, J.-H.; Jeon, Y.-J.; Kim, K. *Nature* **2000**, *404*, 982−986.
(19) Sawaki, T.; Aoyama, Y. *J. Am. Chem. Soc.* **1999**, *121*, 4793−4798.
(20) Albrecht, M.; Lutz, M.; Spek, A. L.; van Koten, G. *Nature* **2000**, *406*, 970−974.
(21) Real, J. A.; Andrés, E.; Muñoz, M. C.; Julve, M.; Granier, T.; Bousseksou, A.; Varret, F. *Science* **1995**, *268*, 265−267.
(22) Beauvais, L. G.; Shores, M. P.; Long, J. R. *J. Am. Chem. Soc.* **2000**, *122*, 2763−2722.
(23) Evans, O. R.; Lin, W. *Chem. Mater.* **2001**, *13*, 2705−2712.
(24) Atwood, J. L.; Barbour, L. J.; Jerga, A.; Schottel, B. L. *Science* **2002**, *298*, 1000−1002.
(25) Kepert, C. J.; Rosseinsky, M. J. *Chem. Commun.* **1999**, 375−376.
(26) (a) We reported the preliminary results at the 89th annual meeting of the Korean Chemical Society, April 2002, abstract p166. (b) While this study was going on, a paper describing the same structure was published: Chae, H. K.; Kim, J.; Friedrichs, O. D.; O'Keefe, M.; Yaghi, O. M. *Angew. Chem., Int. Ed.* **2003**, *42*, 3907−3909.
(27) Dapperheld, S.; Steckhan, E.; Brinkhaus, K.-H. G.; Esch, T. *Chem. Ber.* **1991**, *124*, 2557−2567.
(28) Choi, H. J.; Lee, T. S.; Suh, M. P. *J. Inclusion Phenom. Macrocyclic Chem.* **2001**, *41*, 155−162.
(29) (a) Atkins, P. W. *Physical Chemistry*, 4th ed.; Oxford University Press: Oxford. 1990; pp 885−888. (b) Jang, B.-B.; Lee, K.-P.; Min, D.-H.; Suh, J. *J. Am. Chem. Soc.* **1998**, *120*, 12008−12016.

10.1021/ja043756x CCC: $30.25

surface area than normal zeolites, high thermal stability up to 430 °C, high hydrogen adsorption property (1.9 wt % at 77 K and 1 atm), and guest-dependent luminescence. It even retains its single crystallinity at 400 °C and high vacuum (10^{-5} Torr) to provide completely desolvated crystal. Most interestingly, the framework exhibits reversible dynamic motion with retention of single crystallinity, undergoing significant positional and rotational rearrangements of the molecular components upon removal and rebinding of the guest molecules. Rotational motion in MOF crystals has never been observed previously, to the best of our knowledge, although some other types of crystal dynamics, such as spongelike shrinkage/swelling and sliding motions, have been reported.[1,6,7,24]

Experimental Section

General Methods. All chemicals and solvents used in the syntheses were of reagent grade and used without further purification. Infrared spectra were recorded with a Perkin-Elmer Spectrum One FT/IR spectrophotometer. Elemental analyses were performed by the National Center for Inter-University Research Facilities in Seoul National University. UV/vis spectra were recorded with a Perkin-Elmer Lamda35 UV/vis spectrophotometer. Thermogravimetric analysis (TGA) and differential scanning calorimetry (DSC) were performed at a scan rate of 5 °C/min and 10 °C/min, respectively, using TGA 2050 and DSC 2100 of TA instruments. X-ray powder diffraction (XRPD) data were recorded on a Mac Science M18XHF-22 diffractometer at 50 kV and 100 mA for Cu Kα ($\lambda = 1.54050$ Å) with a scan speed of 5°/min and a step size of 0.02° in 2θ. Emission spectra were recorded with a Jasco FP-6500 spectrofluorometer. Gas chromatographic experiment were conducted by using a HP6890 series GC system that was fitted with a 30 m × 0.32 mm × 0.25 μm cross-linked poly(dimethylsiloxane) capillary column and interfaced with a GC ChemStation. The column temperature was programmed from 80 °C (3 min) to 230 °C at the rate of 75 °C/min. A flame ionization detector was used. Solid ^{13}C NMR spectra were recorded on a Bruker 400 MHz FT-NMR spectrometer at room temperature.

$[Zn_4O(NTB)_2]\cdot 3DEF\cdot EtOH$ (1). H_3NTB was prepared according to the method previously reported.[27] H_3NTB (0.078 g, 2.1×10^{-4} mol) and $Zn(NO_3)_2\cdot 6H_2O$ (0.115 g, 3.87×10^{-4} mol) were dissolved in DEF/EtOH/H_2O (5/3/2 mL), which were placed in a Teflon vessel within the autoclave. The mixture was heated at 110 °C for 24 h and then cooled to room temperature. Pale, greenish yellow rodlike crystals formed, which were filtered, and washed briefly with mother liquor. Yield: 0.101 g (76%). FT-IR for **1** (KBr pellet): $\nu_{O-C=O}$, 1594, 1559, 1548; $\nu_{CH(NTB)}$, 3065; $\nu_{C=O(DEF)}$, 1640, 1656; $\nu_{CH3(DEF)}$, 2975 cm^{-1}. UV/vis (Diffuse reflectance, λ_{max}) = 237, 321, 375(sh), 428(sh) nm. Anal. Calcd for $C_{59}H_{63}N_5O_{17}Zn_4$: C, 51.51; H, 4.62; N, 5.09. Found: C, 51.93; H, 4.47; N, 4.99.

$[Zn_4O(NTB)_2]$ (1′). The single crystal **1** was desolvated on a Quantachrome Autosorb-1 instrument after its X-ray structure was determined. Single-crystal **1** was introduced into a 0.5-mm glass capillary having an open end, which was inserted to a 9-mm cell of the gas sorption apparatus. It was heated at 400 °C under 10^{-5} Torr for 30 min, and then cooled to room temperature, maintaining the high vacuum condition. Removal of all solvent guest molecules was checked by an outgassing test process. The cell was filled with He gas (1.0 atm), and then the capillary was taken out, which was sealed immediately for the X-ray structure determination. For preparation of bulk amount, **1** (45 mg) was desolvated in a Schlenk tube at 220 °C under vacuum for 5 h. FT-IR for **1′** (KBr pellet): $\nu_{O-C=O}$, 1595, 1538; ν_{CH}, 3065 cm^{-1}. Anal. Calcd for $C_{42}H_{24}N_2O_{13}Zn_4$: C, 49.16; H, 2.36; N, 2.73. Found: C, 49.08; H, 2.40; N, 2.88.

$[Zn_4O(NTB)_2]\cdot x DEF\cdot y EtOH$ (1″). The single crystal of **1** was desolvated with a method similar to that for **1′** at 220 °C under 10^{-5} Torr for 10 h. After the X-ray structure of the desolvated crystal was determined, one side of the sealed capillary was broken, and the vapor of mixed solvent DEF/EtOH (3:1, v/v) was allowed to diffuse into the capillary for 12 h to resolvate the crystal. The opening of the capillary was sealed again, and the X-ray structure of **1″** was determined.

Gas Sorption Study. A measured amount of $[Zn_4O(NTB)_2]\cdot 3DEF\cdot EtOH$ (**1**) was introduced into Quantachrome Autosorb-1 gas sorption apparatus, and then the compound was evacuated at 220 °C and 10^{-5} Torr to remove all guest molecules. Nitrogen gas sorption isotherm was monitored at 77 K at each equilibrium pressure by the static volumetric method. Hydrogen gas sorption isotherm was measured by the similar procedure at 77 K.

Guest Binding Study. Pale-yellow crystals of **1** were dried at 220 °C under vacuum for 24 h. The solid (14.8−22.6 mg), whose weight was exactly measured, was immersed in the measured volume of isooctane solutions containing methanol, pyridine, dodecane, and benzene, respectively, for ca. 4 h at 20 °C. The initial concentrations ($[G]_0$) of the guests were varied as 1.17×10^{-2} to 1.06×10^{-1} M for MeOH, 3.09×10^{-2} to 1.98×10^{-1} M for pyridine, 2.87×10^{-2} to 2.09×10^{-1} M for benzene, and 7.33×10^{-2} to 4.93×10^{-1} M for dodecane to keep the saturation (θ) values ranging from 20% to 80%. The concentration change of the organic guest was measured by GC. The formation constant (K_f) for the host−guest complexes formed between a binding site (BS) of the insoluble hosts and a guest molecule (G) was defined as k_{ad}/k_{de} [eqs 1 and 2 by the analogy with Langmuir isotherm for adsorption of gas molecules on solid surfaces.[3a,28,29] The plots of the concentration of G bound to BS ([BS·G]) against [G] were made, and K_f and $[BS]_o/\omega$ values were estimated by the analysis of the data according to eqs 3 and 4.

$$\mathrm{BS} + \mathrm{G} \underset{k_{de}}{\overset{k_{ad}}{\rightleftharpoons}} \mathrm{BS\cdot G} \tag{1}$$

$$K_f = \frac{k_{ad}}{k_{de}} = \frac{[\mathrm{BS\cdot G}]}{[\mathrm{BS}][\mathrm{G}]} \tag{2}$$

If θ is defined as fractional coverage,

$$\theta = \frac{[\mathrm{BS\cdot G}]}{[\mathrm{BS}]_o} = \frac{[\mathrm{G}]}{([\mathrm{G}] + 1/K_f)} \tag{3}$$

then

$$[\mathrm{BS\cdot G}]/\omega = \frac{([\mathrm{BS}]_o/\omega)[\mathrm{G}]}{([\mathrm{G}] + 1/K_f)} \tag{4}$$

where ω is the amount of host solid per unit volume of the solution (mg/mL).

Crystallography. Diffraction data for **1**, **1′**, and **1″** were collected with an Enraf Nonius Kappa CCD diffractometer (Mo Kα, $\lambda = 0.71073$ Å, graphite monochromator). Preliminary orientation matrixes and unit cell parameters were obtained from the peaks of the first 10 frames and then refined using the whole data set. Frames were integrated and corrected for Lorentz and polarization effects using DENZO.[30] The scaling and the global refinement of crystal parameters were performed by SCALEPACK.[30] No absorption correction was made. The crystal structures were solved by the direct method[31] and refined by full-matrix least-squares refinement using the SHELXL-97 computer program.[32] For $Zn_4O(CO_2)_6$ unit in **1** and **1″**, all zinc atoms and all carboxylic oxygen atoms were statistically disordered. The site occupancy factors were given to 0.5 for Zn(1) atom that sits on a general position and 0.1667 for Zn(2) atom that sits on a three-fold crystallographic axis.

(30) Otwinowsky, Z.; Minor, W. *Processing of X-ray Diffraction Data Collected in Oscillation Mode, Methods in Enzymology*; Carter, C. W., Sweet, R. M., Eds.; Academic Press: New York, 1996; Vol. 276, pp 307−326.
(31) Sheldrick, G. M. *Acta Crystallogr*. **1990**, *A46*, 467.
(32) Sheldrick, G. M. "*SHELXL97*, Program for the crystal structure refinement; University of Göettingen: Göettingen, Germany, 1993.

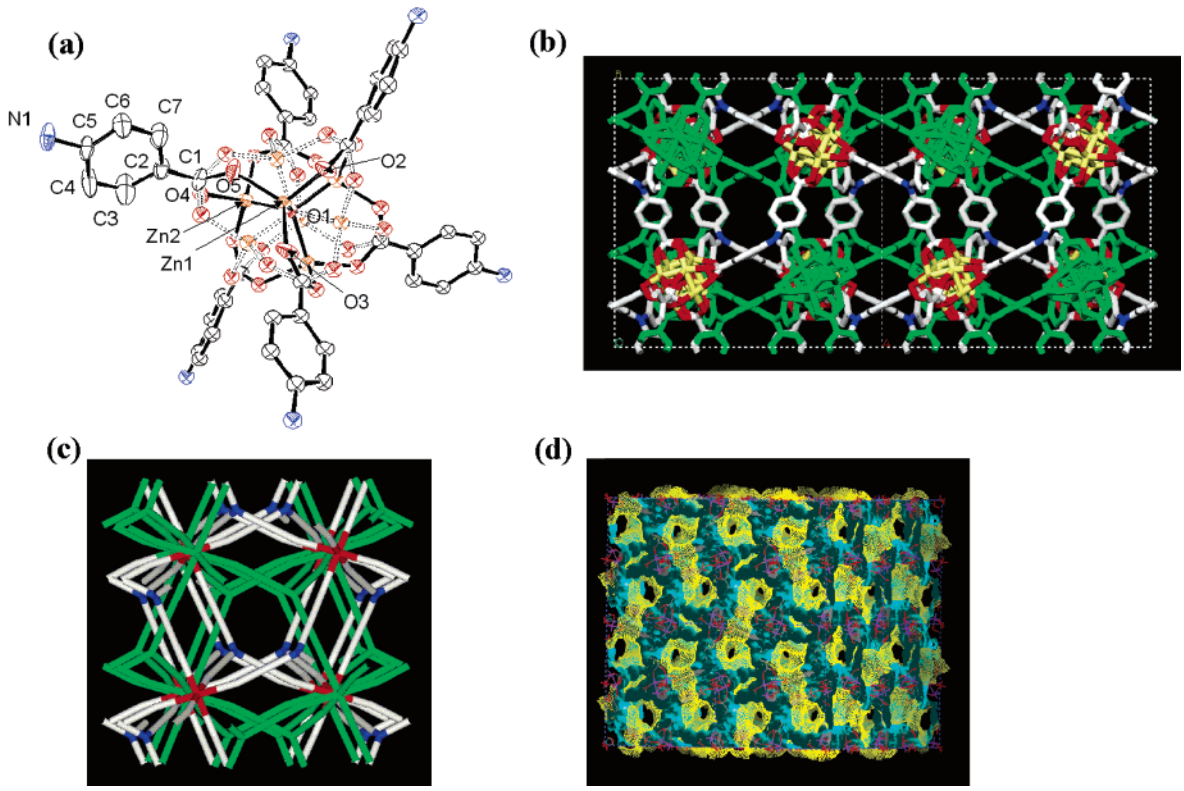

Figure 1. (a) An ORTEP drawing of **1** with the atomic numbering scheme. Thermal ellipsoids are drawn with 30% probability. All carboxylate oxygen atoms and zinc atoms in the $Zn_4O(CO_2)_6$ unit are statistically disordered over two sites, which are described as the dotted lines. (b) 3D network structure of **1**. Zn, yellow; O, red; N, blue; C, gray. Green represents another interpenetrated 3D net. (c) Line drawing of doubly interpenetrated structure of **1**. For simplicity, only the μ_4-oxo atom, the nitrogen of NTB^{3-}, and the carbon atoms (C1, C2 and C5) locating on the line are drawn. Color scheme: red, μ_4-oxygen; blue, N of NTB^{3-}; gray, carbon. Green represents another interpenetrated 3D network. (d) View showing the 3D curved channels of **1**. Zn (violet), oxygen (red), and carbon (gray). Host framework is indicated in blue. The accessible surface in the channels is shown in yellow dots.

Table 1. Comparison of Crystal Structures between **1** and **1′**

	dihedral angles between the planes (deg)				torsion angles of	π–π interactions[d]	
MOF	Zn–O–Zn vs phenyl	Zn–O–Zn vs O–C–O	O–C–O vs phenyl	phenyl vs phenyl[c]	O_{oxo}–Zn–O–C (deg)	C–C[(i)] (Å)	dihedral angle (deg)
1	32.5(2)[a] 60.0(2)[b]	12.4(9)[a] 26.2(14)[b]	20.6(16)[a] 34.7(10)[b]	0.0(4)	22.2(10)[e] 16.0(9)[f] 34.2(11)[g] 53.9(14)[h]	3.917(24)	3.7(4)
1′	25.7(3)[a] 18.0(2)[b]	19.8(3)[a] 15.0(12)[b]	10.3(2)[a] 5.8(10)[b]	84.7(3)	−17.7(2)[e] −19.6(2)[f] 13.0(7)[g] 11.9(10)[h]	3.630(9)	68.3(3)
2 (MOF-150)[26b]	33.2, 59.8	17.9, 28.0	15.7, 31.9	0.0	−27.7, 53.5, 41.8, 28.5	3.957	3.8

[a] Phenyl rings involving Zn1a, Zn1b, O2, and O3. [b] Phenyl rings involving Zn1, Zn2, O4, and O5. [c] Phenyl rings locating at the trans position of octahedron edge around $Zn_4O(CO_2)_6$ cluster. [d] Involving NTB^{3-} ions belonging to two interpenetrated nets. [e] O1−Zn1a−O2−C1a. [f] O1−Zn1b−O3−C1a. [g] O1−Zn2−O4−C1(C8 in **1′**). [h] O1−Zn1−O5−C1(C8 in **1′**). [i] The shortest C- - -C distance.

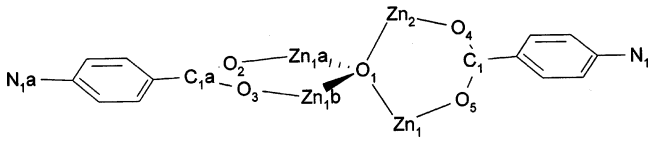

The site occupancy factors were given to 0.5 for all carboxylic oxygen atoms. For desolvated crystal **1′**, no disordered atom was found, contrary to **1**. The positions of all non-hydrogen atoms were refined with anisotropic displacement factors. The hydrogen atoms were positioned geometrically and refined using a riding model. As for the guest molecules of **1**, three residual electron densities, which might correspond to the guest molecule, per asymmetric unit were found with severe disorder. Therefore, the identity and number of the guest molecules (three DEF and one EtOH) in **1** were determined on the basis of IR, elemental analysis, and TGA data. The density of the disordered guest molecule was flattened by using the SQUEEZE option of *PLATON*.[33] The final refinement was made by using the squeezed *hkl* data. For resolvated crystal **1″**, all atoms of the $Zn_4O(CO_2)_6$ cluster were

(33) Spek, A. L. *PLATON99*, A Multipurpose Crystallographic Tool; Utrecht University: Utrecht, The Netherlands, 1999.

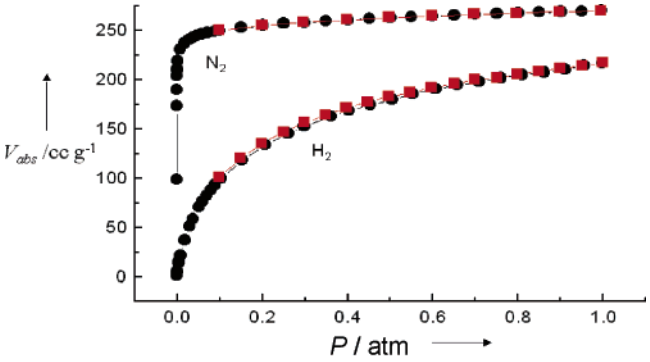

Figure 2. N_2 and H_2 gas sorption isotherms for **1** (■ in red indicates desorption).

disordered with the same site occupancies as those in **1**. However, the residual electron densities corresponding to guest molecules were not observed in **1″** during the refinement process. Crystal data for **1**: cubic, space group Ia-3, $a = 22.541(5)$ Å, $V = 11453(4)$ Å^3, $R_1 = 0.0898$ ($I > 2\sigma(I)$), wR_2 ($I > 2\sigma(I)$) = 0.2815. Crystal data for **1′**: cubic, space group Pa-3, $a = 22.393(5)$ Å, $V = 11229(4)$ Å^3, $R_1 = 0.0720$ ($I > 2\sigma(I)$), wR_2 ($I > 2\sigma(I)$) = 0.1888. Crystal data for **1″**: cubic, space group Ia-3, $a = 22.4509(4)$ Å, $V = 11316.2(3)$ Å^3, $R_1 = 0.0823$ ($I > 2\sigma(I)$), wR_2 ($I > 2\sigma(I)$) = 0.2442. The detailed crystallographic data and bond distances and angles of **1** (squeezed data), **1′**, **1″**, and **1** (raw data) are provided in Tables S1−S12 of Supporting Information.

Results and Discussion

Structure and Properties of $[Zn_4O(NTB)_2]\cdot 3DEF\cdot EtOH$ (1). When $Zn(NO_3)_2\cdot 6H_2O$ and H_3NTB (2:1 mole ratio) were heated at 110 °C in the mixture of DEF/EtOH/H_2O (5:3:2) for 24 h, $[Zn_4O(NTB)_2]\cdot 3DEF\cdot EtOH$ (**1**) was formed. A framework having the same structure as **1**, $[Zn_4(O)(NTB)_2]\cdot 3DMF\cdot 3H_2O$ (**2**, MOF-150), was published previously,[26b] which was prepared from the reaction conditions different from those for **1**: $Zn(NO_3)_2\cdot 6H_2O$ and H_3NTB in the 4.3:1 mole ratio in DMF/EtOH/H_2O (4:1:1, v/v) at 90 °C. It has been frequently observed that the framework structure depends on the reaction conditions such as type of solvent, temperature, and stoichiometry of the reactants even if same molecular building blocks are employed.[2a,15c,34,35] However, structures of **1** and **2** are same even though they are prepared at different reaction conditions and include different guest molecules.

The X-ray structure of **1** is shown in Figure 1. In **1**, the $Zn_4O(CO_2)_6$ cluster acts as an octahedral secondary building unit (SBU), and 4,4′,4″-nitrilotrisbenzoate(NTB^{3-}) acts as a triangular organic building block. A μ_4-oxo bridged Zn_4O tetrahedron cluster is edge-bridged by six carboxylate groups of six NTB^{3-} units to provide the octahedron-shaped SBU, which extends infinitely to give rise to (3,6)-connected nets. The three-dimensional (3D) network is doubly interpenetrated to generate curved 3D channels. The NTB^{3-} looks like a propeller since its phenyl rings are tilted relative to each other with dihedral angles of 69.1(3)°. The central nitrogen of the NTB^{3-} ligand is sp^2 hybridized, showing unusually short N−C distances (1.418(5) Å) and C−N−C angles close to 120°. Some of the key dihedral and torsion angles in **1** are summarized in Table 1. Two phenyl rings of NTB^{3-} ligands located at the trans position of the $Zn_4O(CO_2)_6$ cluster are parallel to each other (dihedral angle, 0.0(4)°), and the N- - -N distance involving these two

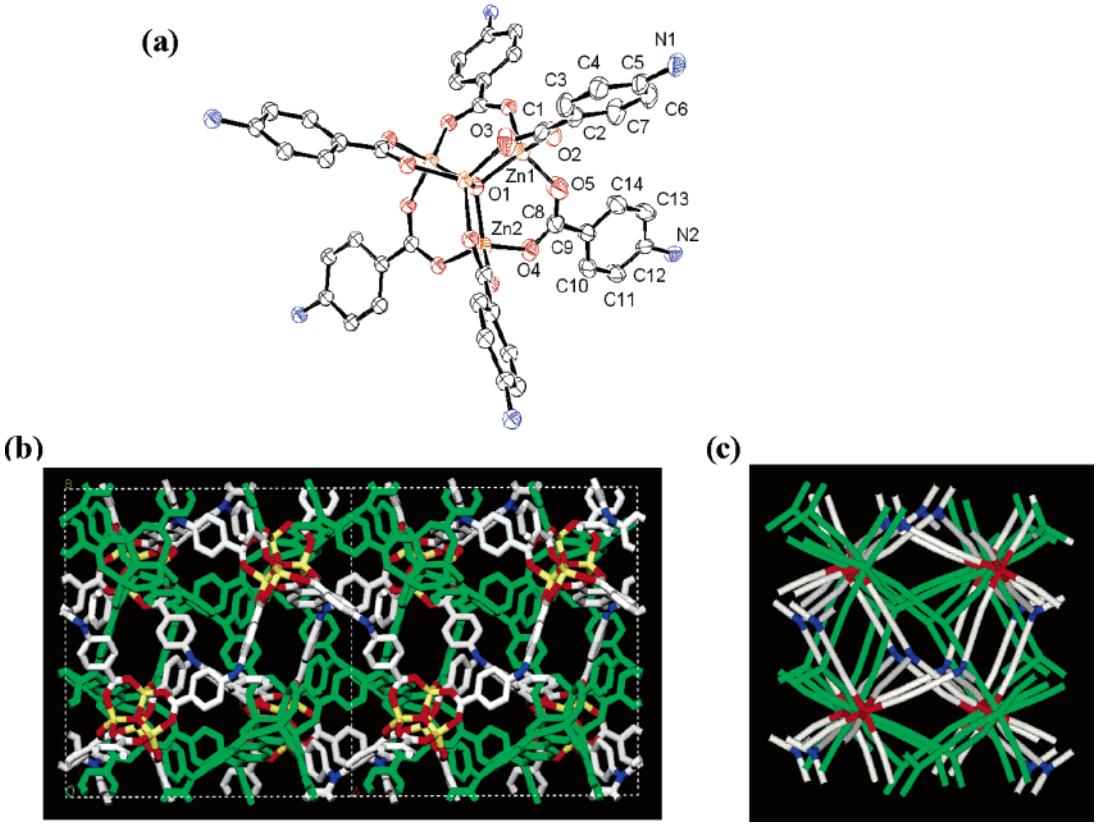

Figure 3. (a) An ORTEP drawing of desolvated compound $[Zn_4O(NTB)_2]$ (**1′**) with the atomic numbering scheme. Thermal ellipsoids are drawn with 30% probability. (b) Doubly interpenetrated 3D network structure of **1′**. (c) Line drawing of doubly interpenetrated structure of **1′**. For simplicity, only the μ_4-oxo atom, the nitrogen of NTB^{3-}, and the carbon atoms [(C1, C2, C5) and (C8, C9, C12)] locating on the line are drawn. Color scheme is same as in Figure 1.

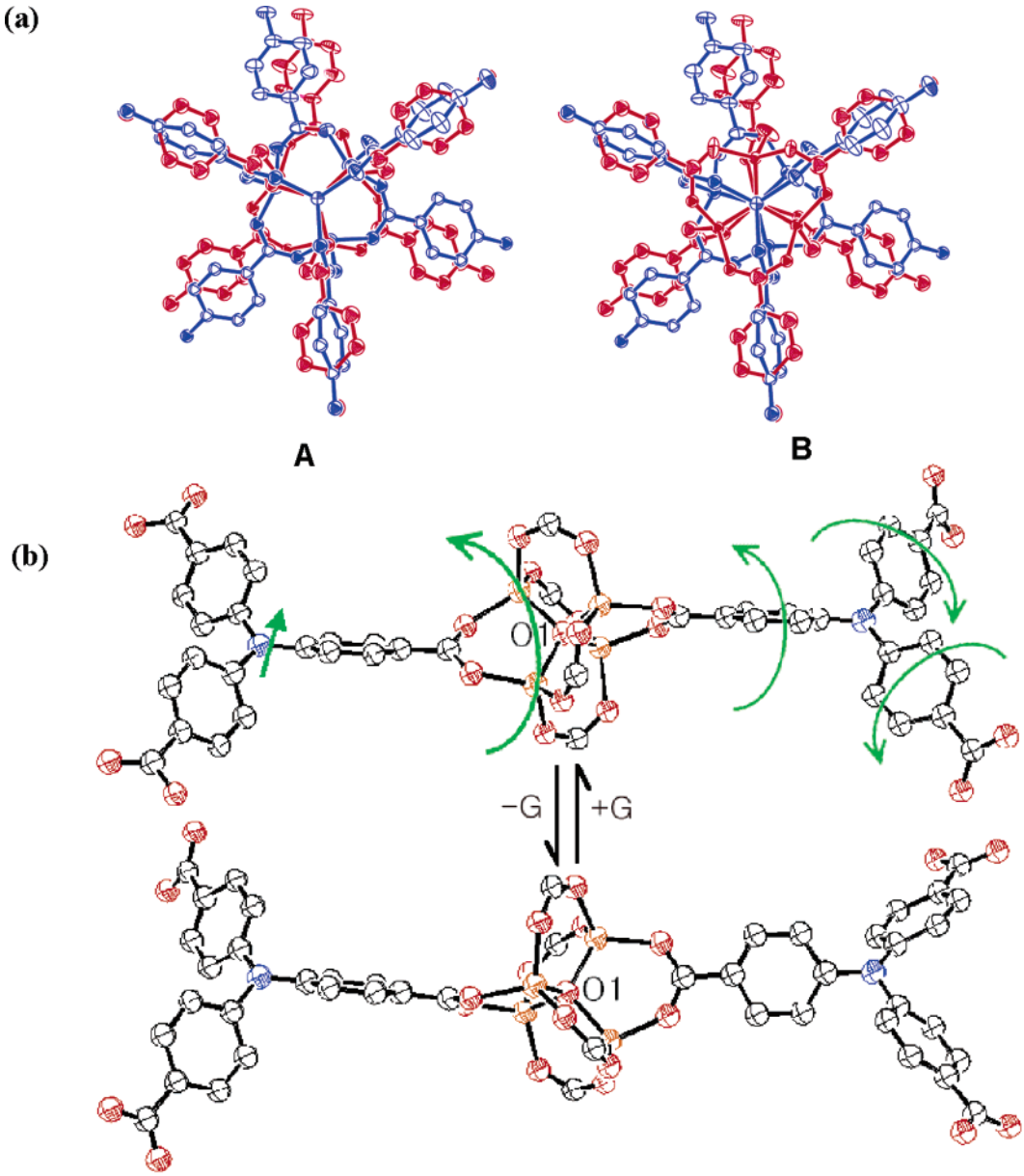

Figure 4. (a) Comparison of the structures between **1** (red) and **1′** (blue). Statistically disordered structures of **1** are separated into two parts (A and B), and each of them is superimposed with the structure of **1′** that is not disordered. The site occupancy factors in **1** were given to 0.5 for all carboxylic oxygen atoms, 0.5 for the Zn atom that sits in a general position, and 0.1667 for the Zn atom that sits on a three-fold crystallographic axis. Thermal ellipsoids are drawn with 30% probability. (b) Rearrangements of the framework components upon guest removal and rebinding. Thermal ellipsoids are drawn with 50% probability. Color scheme: Zn, yellow; O, red; N, blue; C, gray.

NTB^{3-} ligands is 18.451(4) Å. There is no interaction between the phenyl rings of NTB^{3-} belonging to two interpenetrated nets; the shortest C- - -C distance and dihedral angle between the phenyl rings of the adjacent NTB^{3-} units are 3.917(24) Å and 3.7(4)°, respectively. The 3D network structure of **1** can be viewed as a PdF_2-net[36] or an FeS_2-net.[26b,36] The void volume calculated by *PLATON*[33] is 39.7%.

1 is insoluble in water and common organic solvents. Thermal gravimetric analysis reveals 18.2% weight loss at 50−230 °C, corresponding to the loss of one EtOH and two DEF guest molecules per formula unit (calcd 18.0%), followed by additional weight loss of 7.8% at 230−430 °C, corresponding to one DEF guest (calcd 7.4%). The N_2 gas sorption study on the evacuated solid of **1** reveals a reversible type-I isotherm (Figure 2), characteristic of a microporous material. The isotherm shows no hysteresis upon desorption of gas from the pores. The Langmuir surface area and pore volume, estimated by applying the Langmuir and Dubinin−Raduskhvich equations, respectively, are 1121 m^2/g and 0.51 cm^3/cm^3. This compares favorably with zeolites whose pore volume ranges from 0.18 cm^3/cm^3 to 0.47 cm^3/cm^3.[37] A plot of Horvath−Kawazoe (HK) differential pore volume[38] indicates that **1** contains cylindrical pores of ca. 5.0 Å opening in agreement with the X-ray structure. **1** adsorbs H_2 gas up to 1.9 wt % (10 hydrogen molecules per formula unit) at 77 K and 1 atm (Figure 2).[15e,39] This value is notably higher than that of the most favorable zeolite ZSM-5 (0.7 wt %) or those of previously reported $Mn(HCO_2)_2$ (0.9 wt %)[39b] and Yaghi's MOFs (0.89−1.62 wt %),[39c] which were

(34) (a) Li, H.; Eddaoudi, M.; Groy, T. L.; Yaghi, O. M. *J. Am. Chem. Soc.* **1998**, *120*, 8571−8572. (b) Li, H.; Davis, C. E.; Groy, T. L.; Kelley, D. G.; Yaghi, O. M. *J. Am. Chem. Soc.* **1998**, *120*, 2186−2187.
(35) Moulton, B.; Zaworotko, M. *Chem. Rev.* **2001**, *101*, 1629−1658.

measured at 77 K and 1 atm. Because the H_2 sorption isotherm of **1** is not fully saturated at 1 atm, a higher hydrogen sorption capacity may be expected under higher pressures. Therefore, the present compound might be a good candidate for hydrogen storage materials.[15e,39]

Reversible Dynamics of Framework Components with Retention of Single Crystallinity on Desolvation and Resolvation. 1 maintained its single crystallinty as well as transparency even when the single crystal was desolvated at high temperature and high vacuum (400 °C and 10^{-5} Torr) for 0.5 h and provided the single crystal of apohost $[Zn_4O(NTB)_2]$ (**1′**). In general, single crystals of MOFs are frequently broken into small pieces and lose transparency when they are heated or evacuated, although some crystal structures of desolvated solids have been reported.[1,5,6,8,11,13,14,24,25] However, several MOFs could maintain single crystallinity even at high temperature (300 °C)[14a] or reduced pressure (5×10^{-5} Torr),[14b] but never under both conditions as in the present work. Previously, we observed single-crystal-to-single-crystal transformations upon removal and exchange of guest molecules for the bilayered MOF containing flexible pillars.[1] In this case, X-ray structure indicated spongelike shrinkage of the bilayer when the guest molecules were removed.

The X-ray structure of the desolvated crystal (**1′**) is shown in Figure 3. In **1′**, there are two crystallographically different NTB^{3-} ligands around a Zn_4O cluster. Contrary to **1**, **1′** does not contain disordered atoms. The void volume calculated by *PLATON*[33] is 40.1%.

When **1′** is compared with **1** (Figure 4), the local structure of the tetrahedral Zn_4O cluster and the NTB^{3-} unit is very similar to that of **1**. However, the Zn_4O cluster and NTB^{3-} units undergo significant positional and rotational rearrangements upon desolvation by keeping the original positions of the central oxygen atom and the nitrogen atom of one of the two independent NTB^{3-} units. As summarized in Table 1, many of the key dihedral angles in **1′** change significantly compared with those of **1** upon loss of guest molecules. In particular, the dihedral angle in **1′** between two phenyl rings locating at the trans position around the $Zn_4O(CO)_2$ cluster becomes 84.7(3)°, which is remarkably different from that (0°) in **1**.

Figure 4 shows how the framework structure in **1′** is changed relative to that in **1** by separating the statistically disordered structure of **1** into two parts (A and B). In one group of molecules (A), all atoms perform positional rearrangements, except the central oxygen atom of the Zn_4O cluster and the C atoms connected to central nitrogen in one of the two independent NTB^{3-} units. In addition, three phenyl rings around the Zn_4O cluster are rotated with respect to the C−C axes, while the other three phenyl rings are slightly shifted without rotational motion. In the other group of molecules (B), the cluster unit also undergoes rotational motion in addition to these rearrangements. Although there are several crystallographic data showing dynamic behavior upon removal or exchange of guests,[1,6,7,24] the "*rotational motion of the framework components*" in the MOF has never been observed to the best of our knowledge.

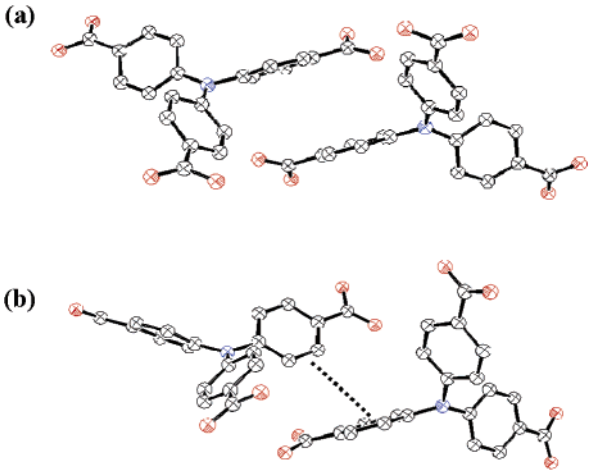

Figure 5. Interactions between the phenyl rings of NTB^{3-} belonging to two independent interpenetrated nets (- - -) in (a) original solid **1** (no interaction) and (b) desolvated solid **1′** (edge-to-face $\pi-\pi$ interaction). Thermal ellipsoids are drawn with 30% probability. Zn, yellow; O, red; N, blue; C, gray.

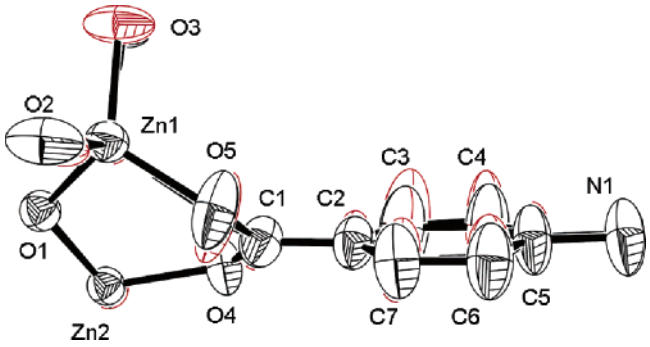

Figure 6. Superimposition of the crystallographic asymmetric units of **1″** (black) and **1** (red).

This crystal dynamics observed in this framework must be triggered by the $\pi-\pi$ interactions between the interpenetrated nets in **1′** (Figure 5), which exhibits edge-to-face $\pi-\pi$ interactions[40] between the phenyl rings belonging to two interpenetrated nets (shortest C− −C distance, 3.630(9) Å; dihedral angle, 68.3(3)°). When the free space is produced in the crystal by guest solvent removal, molecular components undergo significant rearrangements mainly with rotational motion to induce the stronger edge-to-face $\pi-\pi$ interactions. To maintain the original 3D integrity, extensive cooperative motion must occur throughout the crystal.

Interestingly, this crystal dynamic is reversible: when the desolvated crystal was exposed again to the vapor of DEF/EtOH (3:1 v/v) for 12 h (**1″**), the framework structure the same as **1** was restored as evidenced by X-ray crystallography (Figure 6). In **1″,** all atoms of the $Zn_4O(CO_2)_6$ cluster locate at the same positions and are disordered with the same site occupancies as those in **1**. The only difference between **1** and **1″** is that the residual electron densities found in **1**, which might correspond to guest molecules, were not observed in **1″** during the refinement process. Furthermore, when the desolvated crystal (**1′**) was immersed in EtOH, MeOH, pyridine, benzene, or dodecane, the framework structure returned to **1** independent of the type of solvent included.

(36) O'Keeffe, M.; Hyde, B. G. *Crystal Structures, 1: Patterns and Symmetry*; Mineralogical Society of America (U.S.A.), 1996.
(37) Breck, D. W. *Zeolite Molecular Sieves*; Wiley & Sons: New York, 1974.
(38) Horvath, G.; Kawazoe, K. *J. Chem. Eng. Jpn.* **1983**, *16*, 470−475.
(39) (a) Schlapbach, L.; Züttel, A. *Nature* **2001**, *414*, 353−358. (b) Dybtsev, D. N.; Chun, H.; Yoon, S. H.; Kim, D.; Kim, K. *J. Am. Chem. Soc.* **2004**, *126*, 32−33. (c) Rowsell, J. L. C.; Millward, A. R.; Park, K. S.; Yaghi, O. M. *J. Am. Chem. Soc.* **2004**, *126*, 5666−5667.
(40) Desiraju, G. R., Ed. *Perspectives in Supramolecular Chemistry: Crystal as a Supramolecular Entity;* John Wiley & Sons: Chichester, 1996; Vol. 2, pp 168−170.

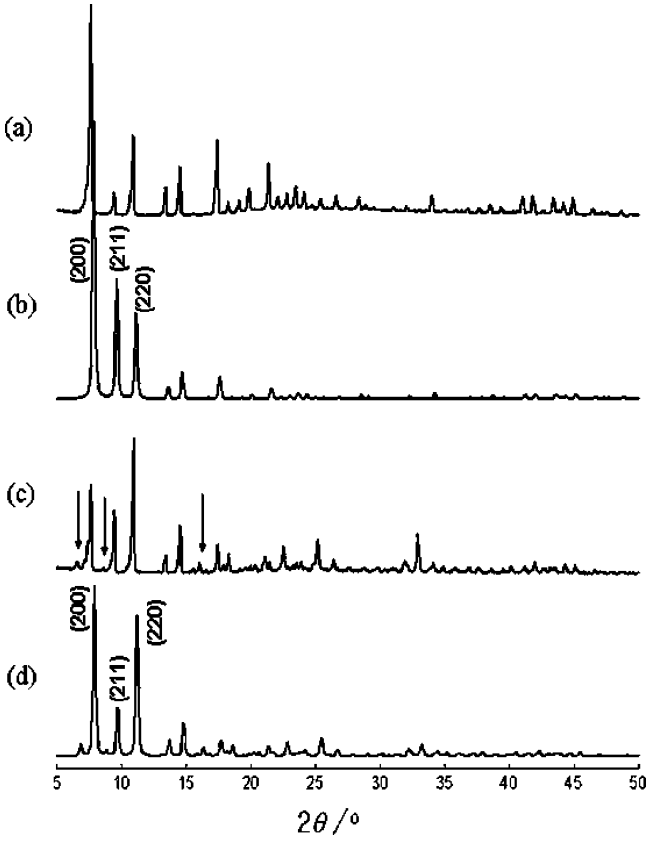

Figure 7. XRPD patterns: (a) for original solid **1**, (b) simulated from the single-crystal X-ray data of **1**, in which electron densities corresponding to the disordered guest molecules were flattened by using the SQUEEZE option of *PLATON*,[33] (c) desolvated solid at 220 °C under vacuum for 24 h (↓ indicates new peak), (d) powder pattern simulated from the single-crystal X-ray data of **1′**. Simulated patterns (b) and (d) are drawn by providing $2\theta = 11.0°$ peaks, similar in intensity to those of (a) and (c), respectively.

XRPD and Solid NMR Spectra. The dynamic motion in the framework is also evidenced by XRPD and solid NMR spectra of **1** and **1′**. The peak positions of the measured XRPD pattern for **1** (Figure 7a) are coincident with those of the simulated pattern (Figure 7b) derived from the X-ray single-crystal data even though the relative intensities are different, indicating that the bulk sample is the same as the single crystal. The difference in the relative intensities between the measured and the simulated patterns for **1** may be attributed to the fact that the measured sample contains guest molecules, while the simulated pattern ignored the guests since single-crystal data employed the SQUEEZE option of the *PLATON* program[33] for the electron densities corresponding to the disordered guest molecules. The XRPD pattern of the desolvated solid **1′** (Figure 7c) indicates that new peaks appear at $2\theta = 6.6, 8.6, 15.5, 16.0°$ and many high-angle peaks ($2\theta > 16°$) are shifted as compared with that of **1**. This indicates that structure changes upon desolvation. The measured XRPD pattern of **1′** is coincident with the simulated pattern (Figure 7d) derived from the single-crystal data of **1′**, implying that the bulk sample dried at 220 °C under vacuum for 24 h has the same structure as the single crystal of **1′**.

The ^{13}C solid NMR spectrum of **1** shows 13 different peaks, five from ligand of the host (a, b, c, d, e; b and e are overlapped) and nine from the solvents (Figure 8). Upon desolvation, the solvent peaks disappear, and all carbon peaks of the NTB^{3-} are shifted. In particular, two (d and e) of five peaks (a−e) for the NTB ligand are split into four (d + d′ and e + e′), indicating

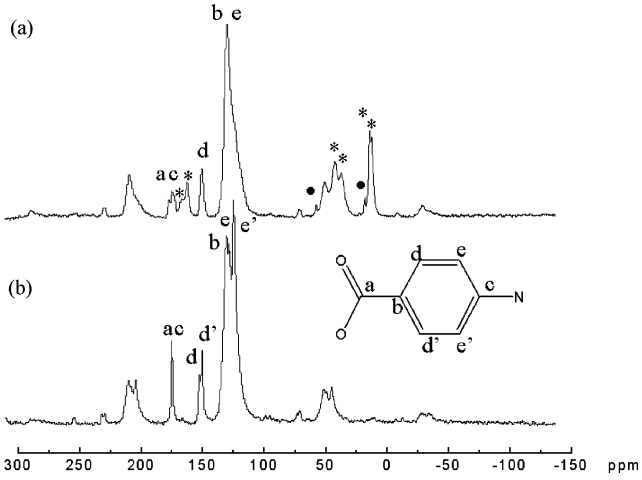

Figure 8. 400 MHz solid-state CP MAS ^{13}C NMR spectra of (a) **1** and (b) **1′** measured at room temperature. (a) a, 177.7; c, 175.4; d, 151.1; b and e, 130.8; CH_3 of DEF, 14.8, 13.1; CH_2 of DEF, 43.1, 37.9; CO of DEF, 167.2, 163.2; CH_3 of EtOH, 58.3; CH_2 of EtOH, 18.8 ppm. Assignments are based on the *ChemDraw* program. (*) indicates two DEF molecules in different environments and (●) indicates EtOH. Unnoted peaks are sidebands. (b) a, 176.2; c, 176.2; d, 153.2; d′, 150.9; b and e, 131.2; e′, 129.3 ppm.

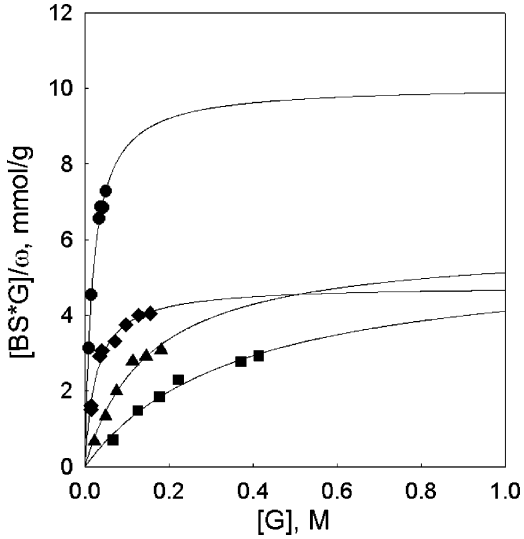

Figure 9. Binding of host solid **1′** with organic guests. MeOH (●), pyridine (◆), benzene (▲), and dodecane (■).

that the chemical environment of the two carbon atoms (d and e) of the phenyl ring is changed, which is coincident with the X-ray structure of **1′** exhibiting the rotational rearrangement of phenyl rings in the host.

Guest Binding of Desolvated Solid 1′. The desolvated host solid **1′** binds methanol, pyridine, benzene, and dodecane in the isooctane medium, exhibiting Langmuir isotherm curves (Figure 9). The amount of the guest bound to the host solid was measured by GC, and the formation constant (K_f) and the number of binding sites (mol) per g of the host ($[BS]_o/\omega$) for guest molecules were estimated (Table 2). The host differentiates organic guests with the K_f values in the order of MeOH > pyridine > benzene > dodecane. It is evident that the host favors the guests that are able to form hydrogen bonds with its carbonyl groups exposed to the channels.[2c,3a,28] In addition, it favors the hydrophobic guests because of the benzyl rings contained in the host that might induce $\pi-\pi$ or C−H- - -π interactions with the guest molecules.

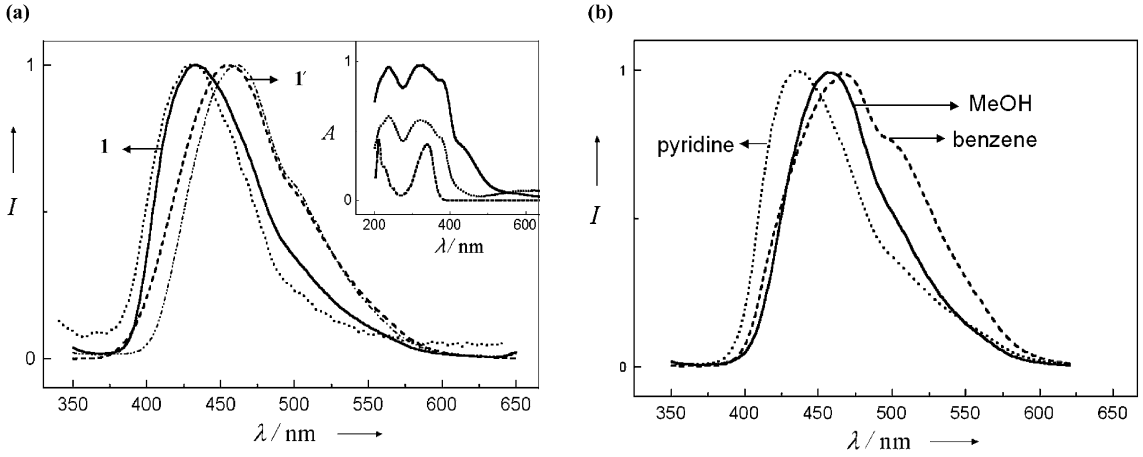

Figure 10. (a) Luminescent spectra: **1** (—), **1′** (-···-··-···), solid Na_3NTB (···), and the 0.1 M NaOH solution of H_3NTB (- - -). (Inset) Absorption spectra of **1** (—, λ_{max} = 237, 321, 375(sh), and 428(sh) nm), solid Na_3NTB (···, λ_{max} = 237, 321, and 375(sh) nm), and the 0.1 M NaOH solution of H_3NTB (- - -, λ_{max} = 340 nm). (b) Guest-dependent luminescent spectra with normalized intensity: pyridine (···, λ_{max} = 435 nm), methanol (—, λ_{max} = 456 nm), and benzene (- - -, λ_{max} = 466 nm).

Table 2. Guest Binding Data for Desolvated Framework **1′**

	K_f, M^{-1}	$[BS]_0/\omega$, mmol/g	no. of guest molecules/ unit formula of host
(a) MeOH	52.9	10.1	10
(b) pyridine	37.6	4.79	5
(c) benzene	6.68	5.90	6
(d) dodecane	2.74	4.83	5.5

Guest-Dependent Photo-Luminescence. The host framework exhibits photoluminescence, but λ_{max} depends on the presence or absence of the guest molecules. That is, **1** and **1′** exhibit intense photoluminescence at λ_{max} = 433 nm and λ_{max} = 463 nm, respectively, upon photoexcitation at 340 nm (Figure 10). The 30 nm difference in the luminescence spectra between **1** and **1′** may be attributed to the absence and presence of $\pi-\pi$ interactions, respectively, between the interpenetrated nets. These luminescence spectra are comparable to those of solid Na_3NTB that emits at 430 nm and the 0.1 M NaOH solution of H_3NTB that emits at λ_{max} = 456 nm. It has been reported that luminescent bands are blue-shifted in the solid state compared with those in the solution.[41] For the NTB ligand, blue-shift is also observed in the solid state. The luminescences of **1** and **1′** seem to be originating from the respective ligands. However, the possibility of originating from the Zn_4O cluster cannot be excluded because some zinc clusters emit LMCT luminescence around 420−450 nm.[42] Interestingly, the luminescence also depends on the guest identity (Figure 10b). When desolvated solid **1′** was immersed in the solvent such as pyridine, methanol, and benzene, the respective λ_{max} of the luminescence band appears at different wavelengths, depending on the type of solvent used (435 nm for pyridine, 456 nm for methanol, and 466 nm for benzene). The guest-dependent luminescence shows no relationship with the binding constant of the host with the guest. This guest-dependent luminescence property implies that the present porous material may be applied as a sensor for organic molecules.

In conclusion, we have prepared a porous metal−organic framework consisting of Zn(II) and NTB^{3-}, $[Zn_4O(NTB)_2]\cdot 3DEF\cdot EtOH$ (**1**), in which two independent (3,6)-connected nets are interpenetrated to generate curved 3D channels, and we explored its multifunctionality. **1** shows permanent high porosity, high thermal stability, high hydrogen adsorption capacity, selective organic guest binding ability, and guest-dependent luminescence. Maintaining single crystallinity even at 400 °C and 10^{-5} Torr, the framework components undergo reversible dynamics with positional and *rotational* rearrangements in response to removal and rebinding of the guest molecules. Due to these interesting multifunctionalities and reversible crystal dynamics, the solid might be used as the hydrogen storage material as well as the guest sensor.

Acknowledgment. This work was supported by Ministry of Commerce, Industry, and Energy (project no. M1-0213-03-0001).

Supporting Information Available: TGA/DSC trace of **1**, photographs for crystals, ORTEP drawings of **1″**, and tables of X-ray data for **1** (based on the squeezed data as well as the raw data), **1′,** and **1″**. X-ray crystallographic files in CIF format. This material is available free of charge via the Internet at http://pubs.acs.org.

JA043756X

(41) Sun, S. S.; Lees, A. J. *Coord. Chem. Rev.* **2002**, *230*, 171−192.
(42) (a) Chen, W.; Wang, J. Y.; Chen, C.; Yue, Q.; Yuan, H. M.; Chen, J. S.; Wang, S. N. *Inorg. Chem.* **2003**, *42*, 944−946. (b) Tao, J.; Shi, J. X.; Tong, M. L.; Zhang, X. X.; Chen, X. M. *Inorg. Chem.* **2001**, *40*, 6328−6330. (c) Tao, J.; Tong, M. L.; Shi, J. X.; Chen, X. M.; Ng, S. W. *Chem. Commun.* **2000**, 2043−2044.